

1 **Accelerated hydrological cycle over the Sanjiangyuan region induces**
2 **more streamflow extremes at different global warming levels**

3

4 Peng Ji^{1,2}, Xing Yuan³, Feng Ma³, Ming Pan⁴

5

6 ¹Key Laboratory of Regional Climate-Environment for Temperate East Asia, Institute
7 of Atmospheric Physics, Chinese Academy of Sciences, Beijing 100029, China

8 ²College of Earth and Planetary Sciences, University of Chinese Academy of Sciences,
9 Beijing 1000493, China

10 ³School of Hydrology and Water Resources, Nanjing University of Information
11 Science and Technology, Nanjing 210044, China

12 ⁴Department of Civil and Environmental Engineering, Princeton University, Princeton,
13 New Jersey, USA

14

15 *Correspondence to:* Xing Yuan (xyuan@nuist.edu.cn)

16 **Abstract.** Serving source water for the Yellow, Yangtze and Lancang-Mekong rivers,
17 the Sanjiangyuan region concerns ~700 million people over its downstream areas.
18 Recent research suggests that the Sanjiangyuan region will become wetter in a
19 warming future, but future changes in streamflow extremes remain unclear due to the
20 complex hydrological processes over high-land areas and limited knowledge of the
21 influences of land cover change and CO₂ physiological forcing. Based on high
22 resolution land surface modeling during 1979~2100 driven by the climate and
23 ecological projections from 11 newly released Coupled Model Intercomparison
24 Project Phase 6 (CMIP6) climate models, we show that different accelerating rates of
25 precipitation and evapotranspiration at 1.5°C global warming level induce 55% more
26 dry extremes over Yellow river and 138% more wet extremes over Yangtze river
27 headwaters compared with the reference period (1985~2014). An additional 0.5°C
28 warming leads to a further nonlinear and more significant increase for both dry
29 extremes over Yellow river (22%) and wet extremes over Yangtze river (64%). The
30 combined role of CO₂ physiological forcing and vegetation greening, which used to
31 be neglected in hydrological projections, is found to alleviate dry extremes at 1.5 and
32 2.0°C warming levels but to intensify dry extremes at 3.0°C warming level. Moreover,
33 vegetation greening contributes half of the differences between 1.5 and 3.0°C
34 warming levels. This study emphasizes the importance of ecological processes in
35 determining future changes in streamflow extremes, and suggests a “dry gets drier,
36 wet gets wetter” condition over headwaters.

37 **Keywords** Terrestrial hydrological cycle, streamflow extremes, global warming levels,

39 1 Introduction

40 Global temperature has ~~been~~increasinged at a rate of 1.7°C/decade since 1970,
41 contrary to the cooling trend over the past 8000 years (Marcott et al., 2013). The
42 temperature measurements suggest that 2015-2019 is the warmest five years and
43 2010-2019 is also the warmest decade since 1850 (WMO, 2020). To mitigate the
44 impact of this unprecedented warming on the global environment and human society,
45 195 nations adopted the Paris Agreement which decides to “hold the increase in the
46 global average temperature to well below 2°C above pre-industrial levels and pursuing
47 efforts to limit the temperature increase to 1.5°C”.

48 The response of regional and global terrestrial hydrological processes, including
49 streamflow and its extremes, to different global warming levels has been investigated
50 by numerous studies in recent years (Chen et al., 2017; Döll et al., 2018; Marx et al.,
51 2018; Mohammed et al., 2017; Thober et al., 2018; Zhang et al., 2016). In addition to
52 climate change, recent works reveal the importance of ~~However,~~ the ecological factors
53 (e.g., the CO₂ physiological forcing and land cover change) in modulating the
54 streamflow and its extremes ~~whose importance in modulating the terrestrial~~
55 ~~hydrological responses is emphasized by recent research,~~ ~~are often unaccounted for~~
56 ~~in studies regarding the changes in hydrological extremes.~~ For example, the
57 increasing CO₂ concentration is found to alleviate the decreasing trend of future
58 streamflow at global scale through decreasing the vegetation transpiration by reducing
59 the stomatal conductance (known as the CO₂ physiological forcing) (Fowler et al.,
60 2019; Wiltshire et al., 2013; Yang et al., 2019; Zhu et al., 2012). ~~the suppression of~~

61 ~~stomatal conductance (thus vegetation transpiration) by increased CO₂ concentration~~
62 ~~(known as the CO₂ physiological forcing), is found to alleviate the decreasing trend of~~
63 ~~streamflow in the future at global scale (Wiltshire et al., 2013; Yang et al., 2019; Zhu~~
64 ~~et al., 2012). While~~Contrary to the CO₂ physiological forcing, the vegetation greening
65 in a warming climate is found to have a significant role ~~o~~in exacerbating hydrological
66 drought, as it enhances transpiration and dries up the land (Yuan et al., 2018b).
67 However, the relative contributions of CO₂ physiological forcing and vegetation
68 greening to the changes in terrestrial hydrology especially the streamflow extremes
69 are still unknown, and whether~~Thus, it is necessary to assess~~ their combined impacts
70 ~~on the projection of streamflow extremes~~ changes at different warming levels needs to
71 be investigated.

72 Hosting the headwaters of the Yellow river, the Yangtze river and the
73 Lancang-Mekong river, the Sanjiangyuan region is ~~also~~ known as the “Asian Water
74 Tower” and concerns 700 million people over its downstream areas. Changes in
75 streamflow and its extremes over the Sanjiangyuan region not only influence the local
76 ecosystems, environment and water resources, but also affect the security of food,
77 energy, and water over the downstream areas. Both the regional climate and
78 ecosystems show significant changes over the Sanjiangyuan region due to global
79 warming (Bibi et al., 2018; Kuang and Jiao, 2016; Liang et al., 2013; Yang et al., 2013;
80 Zhu et al., 2016), which makes it a sound region to investigate the role of climate
81 change and ecological change (e.g., land cover change and CO₂ physiological forcing)
82 in influencing the streamflow and its extremes (Cuo et al., 2014; Ji and Yuan, 2018;

83 ~~Zhu et al., 2013). The global warming has induced significant changes in the~~
84 ~~regional alpine climate and fragile ecosystem over~~ make the Sanjiangyuan region
85 sensitive to the global warming (Kuang and Jiao, 2016; Liang et al., 2013; ~~Sadia et~~
86 ~~al., 2018; Yang et al., 2013; Zhu et al., 2016), which then alters the regional~~
87 ~~streamflow and its extremes (Cuo et al., 2014; Ji and Yuan, 2018; Fowler et al., 2019;~~
88 ~~Zhu et al., 2013). For example, H~~historical changes in climate and ecology (e.g. land
89 cover) have significantly altered the terrestrial hydrology and its extremes (Ji and
90 Yuan, 2018; Yuan et al., 2018a). For example, the Yellow river headwater region,
91 which provides more than one-third of the total streamflow in the Yellow river,
92 ~~experienced~~ are found to cause significant reduction in mean and high flows during
93 1979-2005, which potentially ~~increas~~ esing drought risk over its downstream areas (Ji
94 and Yuan, 2018). And the CO₂ physiological forcing is revealed to cause equally large
95 changes in regional flood extremes as the precipitation over the Yangtze and Mekong
96 rivers (Fowler et al., 2019). Recent research suggests that the Sanjiangyuan region
97 will become warmer and wetter in the future, and extreme precipitation will also
98 increase at the 1.5°C global warming level and further intensify with a 0.5°C
99 additional warming (Li et al., 2018; Zhao et al., 2019). However, how the streamflow
100 extremes would respond to the 1.5°C warming, what an additional 0.5°C or even
101 greater warming would cause, and how much contributions do the ecological factors
102 (e.g., CO₂ physiological forcing and land cover change) have, are still unknown. This
103 makes it difficult to assess the climate and ecological impact on this vital headwaters
104 region.

105 In this study, we investigate the future changes in the streamflow extremes over
106 the Sanjiangyuan region from an integrated eco-hydrological perspective by taking
107 CO₂ physiological forcing and land cover change into consideration. The combined
108 impacts of the above two ecological factors at different global warming levels are also
109 quantified and compared with the impact of climate change. The results will help
110 understand the role of ecological factors in future terrestrial hydrological changes
111 over the headwater regions like the Sanjiangyuan, and provide guidance and support
112 for the stakeholders to make relevant decisions and plans.

113 **2 Data and methods**

114 **2.1 Study domain and Observational Data**

115 The Sanjiangyuan region is located at the eastern part of the Tibetan Plateau
116 (Figure 1a), with the total area and mean elevation being 3.61×10^5 km² and 5000 m
117 respectively. It plays a critical role in providing freshwater, by contributing 35%, 20%
118 and 8% to the total annual streamflow of the Yellow, Yangtze and Lancang-Mekong
119 rivers (Li et al., 2017; Liang et al., 2013). The source regions of Yellow, Yangtze and
120 Lancang-Mekong rivers account for 46%, 44% and 10% of the total area of the
121 Sanjiangyuan individually, and the Yellow river source region has a warmer climate
122 and sparser snow cover than the Yangtze river source region.

123 Monthly sStreamflow observations from the Tangnaihai (TNH) and the
124 Zhimenda (ZMD) hydrological stations (Figure 1a), which were provided by the local
125 authorities, were used to evaluate the streamflow simulations. Data periods are
126 1979-2011 and 1980-2008 for the Tangnaihai and Zhimenda stations individually.

127 Monthly terrestrial water storage change observation and its uncertainty during
128 2003-2014 was provided by the Jet Propulsion Laboratory (JPL), which used the mass
129 concentration blocks (mascons) basis functions to fit the Gravity Recovery and
130 Climate Experiment (GRACE) satellite's inter-satellite ranging observations (Watkins
131 et al., 2015). The Model Tree Ensemble evapotranspiration (MTE_ET; Jung et al.,
132 2009) and the Global Land Evaporation Amsterdam Model evapotranspiration
133 (GLEAM_ET) version 3.3a (Martens et al., 2017) were also used to evaluate the
134 model performance on ET simulation.

135 **2.2 CMIP6 Data**

136 Here, 19 Coupled Model Intercomparison Project phase 6 (CMIP6, Eyring et al.,
137 2016) models which provide precipitation, near-surface temperature, specific
138 humidity, 10-m wind speed, surface downward shortwave and longwave radiations at
139 daily timescale were first selected for evaluation. Then, ~~models 11 of them~~ were
140 chosen for the analysis when the simulated as meteorological forcings (e.g.,
141 precipitation, temperature, humidity, and shortwave radiation) averaged over the
142 Sanjiangyuan region they have the same trend signs as the observations during
143 1979-2014. Table 1 shows the 11 CMIP6 models that were finally chosen in this
144 study can best reproduce the increasing precipitation over the Sanjiangyuan region
145 during 1979-2014 (Table 1). For the future projection (2015-2100), we chose two
146 Shared Socioeconomic Pathways (SSP) experiments: SSP585 and SSP245. SSP585
147 combines the fossil-fueled development socioeconomic pathway and 8.5W/m² forcing
148 pathway (RCP8.5), while SSP245 combines the moderate development

149 socioeconomic pathway and 4.5 W/m² forcing pathway (RCP4.5) (O'Neill et al.,
150 2016). Land cover change is quantified by leaf area index (LAI) as there is no
151 significant transition between different vegetation types (not shown) according to the
152 Land-use Harmonization 2 (LUH2) dataset
153 (<https://esgf-node.llnl.gov/search/input4mips/>). For the CNRM-CM6-1, FGOALS-g3
154 and CESM2, the ensemble mean of LAI simulations from the other 8 CMIP6 models
155 was used because CNRM-CM6-1 and FGOALS-g3 do not provide dynamic LAI
156 while the CESM2 simulates an abnormally large LAI over the Sanjiangyuan region.
157 To avoid systematic bias in meteorological forcing, the trend-preserved bias
158 correction method suggested by ISI-MIP (Hempel et al., 2013), was applied to the
159 CMIP6 model simulations at monthly scale. The China Meteorological Forcing
160 Dataset (CMFD) is taken as meteorological observation (He et al., 2020). For each
161 month, temperature bias in CMIP6 simulations during 1979-2014 was directly
162 deducted. Future temperature simulations in SSP245 and SSP585 experiments were
163 also adjusted according to the historical bias. Other variables were corrected by using
164 a multiplicative factor, which was calculated by using observations to divide
165 simulation during 1979-2014. In addition, monthly leaf area index was also adjusted
166 to be consistent with satellite observation using the same method as temperature. All
167 variables were first interpolated to the 10_km resolution over the Sanjiangyuan region
168 and the bias correction was performed for each CMIP6 model at each grid. After bias
169 correction, absolute changes of temperature and leaf area index, and relative changes
170 of other variables were preserved at monthly time scale (Hempel et al., 2013). Then,

171 the adjusted CMIP6 daily meteorological forcings were disaggregated into hourly
172 using the diurnal cycle ratios from the China Meteorological Forcing Dataset ~~(CMFD;~~
173 ~~He et al., 2020).~~

174 The historical CO₂ concentration used here is the same as the CMIP6 historical
175 experiment (Meinshausen et al., 2017), while future CO₂ concentration in SSP245 and
176 SSP585 scenarios came from simulations of a reduced-complexity carbon-cycle
177 model MAGICC7.0 (Meinshausen et al.,
178 ~~2020~~<http://greenhousegases.science.unimelb.edu.au/>).

179 2.3 Experimental design

180 The land surface model used in this study is the Conjunctive Surface-Subsurface
181 Process model version 2 (CSSPv2), ~~which has been proved to simulate the energy and~~
182 ~~water processes over the Sanjiangyuan region well~~ (Yuan et al., 2018a). ~~Figure 2~~
183 ~~shows the structure and main ecohydrological processes in CSSPv2.~~ The CSSPv2 ~~is~~
184 ~~rooted in the Common Land Model (CoLM; Dai et al., 2003) with some~~
185 ~~improvements at hydrological processes. CSSPv2 has a volume-averaged soil~~
186 ~~moisture transport (VAST) model, which solves the quasi-three dimensional~~
187 ~~transportation of the soil water and explicitly considers the variability of moisture flux~~
188 ~~due to subgrid topographic variations (Choi et al., 2007). Moreover, the Variable~~
189 ~~Infiltration Capacity runoff scheme (Liang et al., 1994), and the influences of soil~~
190 ~~organic matters on soil hydrological properties were incorporated into the CSSPv2 by~~
191 ~~Yuan et al. (2018a), to improve its performance in simulating the terrestrial hydrology~~
192 ~~over the Sanjiangyuan region., incorporates the variable infiltration capacity runoff~~

193 ~~scheme, and considers hydrological influences of soil organic matters. Similar to~~
194 ~~CoLM and Community Land Model (Oleson et al., 2013), vegetation transpiration in~~
195 ~~CSSPv2 is based on Monin-Obukhov similarity theory, and the transpiration rate is~~
196 ~~constrained by leaf boundary layer and stomatal conductances. Systematic evaluation~~
197 ~~has proved that CSSPv2 well simulates the energy and water processes over the~~
198 ~~Sanjiangyuan region (Yuan et al., 2018a).~~ Parameterization of the stomatal
199 conductance (g_s) in CSSPv2 is

$$200 \quad g_s = m \frac{A_n}{\frac{P_{CO_2}}{P_{atm}}} h_s + b \beta_t$$

201 where the m is a plant functional type dependent parameter, A_n is leaf net
202 photosynthesis ($\mu mol CO_2 m^{-2} s^{-1}$), P_{CO_2} is the CO_2 partial pressure at the leaf
203 surface (Pa), P_{atm} is the atmospheric pressure (Pa), h_s is the leaf surface
204 humidity, b is the minimum stomatal conductance ($\mu mol m^{-2} s^{-1}$), while β_t is the
205 soil water stress function. ~~This parameterization is also used in the Community Land~~
206 ~~Surface Model (CLM) and the Common Land Surface Model (CoLM).~~ Generally, the
207 stomatal conductance decreases with the increasing of CO_2 concentration.

208 First, bias-corrected meteorological forcings from CMIP6 historical experiment
209 were used to drive the CSSPv2 model (CMIP6_His/CSSPv2). All simulations were
210 conducted for two cycles during 1979-2014 at half-hourly time step and 10 km spatial
211 resolution, with the first cycle serving as the spin-up. Correlation coefficient (CC) and
212 root mean squared error (RMSE) were calculated for validating the simulated monthly
213 streamflow, annual evapotranspiration and monthly terrestrial water storage. The
214 King-Gupta efficiency (KGE; Gupta et al., 2009), which is widely used in streamflow

215 evaluations, was also calculated. Above metrics were calculated as follows:

$$216 \quad CC = \frac{\sum_{i=1}^n (x_i - \bar{x})(y_i - \bar{y})}{\sqrt{\sum_{i=1}^n (x_i - \bar{x})^2 \sum_{i=1}^n (y_i - \bar{y})^2}}$$

$$217 \quad RMSE = \sqrt{\frac{\sum_{i=1}^n (x_i - y_i)^2}{n}}$$

$$218 \quad KGE = 1 - \sqrt{(1 - CC)^2 + (1 - \frac{\sigma_x}{\sigma_y})^2 + (1 - \frac{\bar{x}}{\bar{y}})^2}$$

219 where x_i and y_i are observed and simulated variables in a specific month/year i
220 individually, and \bar{x} and \bar{y} are the corresponding monthly/annual means during the
221 evaluation period n . The σ_x and σ_y are standard deviations for observed and
222 simulated variables, respectively. The KGE ranges from negative infinity to 1, and
223 model simulations can be regard as satisfactory when the KGE is larger than 0.5
224 (Moriasi et al., 2007).

225 Second, bias-corrected meteorological forcings in SSP245 and SSP585 were
226 used to drive CSSPv2 during 2015-2100 with dynamic LAI and CO₂ concentration
227 (CMIP6_SSP/CSSPv2). Initial conditions of CMIP6_SSP/CSSPv2 came from the last
228 year in CMIP6_His/CSSPv2.

229 Then, the second step was repeated twice by fixing the monthly LAI
230 (CMIP6_SSP/CSSPv2_FixLAI) and mean CO₂ concentration
231 (CMIP6_SSP/CSSPv2_FixCO2) at 2014 level. The difference between
232 CMIP6_SSP/CSSPv2 and CMIP6_SSP/CSSPv2_FixLAI is regarded as the net effect
233 of land cover change, and the difference between CMIP6_SSP/CSSPv2 and

234 CMIP6_SSP/CSSPv2_FixCO2 is regarded as the net effect of CO₂ physiological
235 forcing.

236 **2.4 Warming level determination**

237 A widely used time-sampling method was adopted to determine the periods of
238 different global warming levels (Chen et al., 2017; Döll et al., 2018; Marx et al., 2018;
239 Mohammed et al., 2017; Thober et al., 2018). According to the HadCRUT4 dataset
240 (Morice et al., 2012), the global mean surface temperature has increased by 0.66°C
241 from the pre-industrial era (1850-1900) to the reference period defined as 1985-2014.
242 Then, starting from 2015, 30-years running mean global temperatures were compared
243 to those of the 1985-2014 period for each GCM simulation. And the
244 1.5°C/2.0°C/3.0°C warming period is defined as the 30-years period when the
245 0.84°C/1.34°C/2.34°C global warming, compared with the reference period
246 (1985-2014), is first reached. The median years of identified 30-year periods, referred
247 as “crossing years”, are shown in Table 2.

248 **2.5 Definition of dry and wet extremes and robustness assessment**

249 In this research, the standardized streamflow index (SSI) was used to define dry
250 and wet extremes (Vicente-Serrano et al., 2012; Yuan et al., 2017). A gamma
251 distribution was first fitted using July-September (flood season) mean streamflow
252 during the reference period. Then the fitted distribution was used to calculate the
253 standardized deviation of the July-September mean streamflow (i.e. SSI) in each year
254 during both the reference and projection periods. Here, dry and wet extremes were
255 defined as where SSIs are smaller than -1.28 (a probability of 10%) and larger than

256 1.28 respectively.

257 The relative changes in frequency of dry/wet extremes between the reference
258 period and different warming periods were first calculated for each GCM under each
259 SSP scenario, and the ensemble means were then determined for each warming level.
260 To quantify the uncertainty, the above calculations were repeated by using the
261 bootstrap 10,000 times, and 11 GCMs were resampled with replacement during each
262 bootstrap (Christopher et al., 2018). The 5% and 95% percentiles of the total 10,000
263 estimations were finally taken as the 5~95% uncertainty ranges.

264 **3 Results**

265 **3.1 Terrestrial hydrological changes at different warming levels**

266 As shown in Figures 1b-1e, observations (pink lines) show that the annual
267 temperature, precipitation and growing season LAI increase at the rates of
268 0.63°C/decade (p=0), 16.9 mm/decade (p=0.02), and 0.02 m²/m²/decade (p=0.001)
269 during 1979-2014 respectively. The ensemble means of CMIP6 simulations (black
270 lines) can generally capture the historical increasing trends of temperature
271 (0.30 °C/decade, p=0), precipitation (7.1 mm/decade, p=0) and growing season LAI
272 (0.029 m²/m²/decade, p=0), although the trends for precipitation and temperature are
273 underestimated. for growing season LAI (pink lines) reasonably well. In 2015-2100,
274 the SSP245 scenario (blue lines) shows continued warming, wetting and greening
275 trends, and the trends are larger in the SSP585 scenario (red lines). The CO₂
276 concentration also keeps increasing during 2015-2100 and reaches to 600 ppm and
277 1150 ppm in 2100 for the SSP245 and SSP585 scenarios respectively. Although the

278 SSP585 scenario reaches the same warming levels earlier than the SSP245 scenario
279 (Table 2), there is no significant difference between them in the meteorological
280 variables during the same warming period (not shown). Thus, we do not distinguish
281 SSP245 and SSP585 scenarios at the same warming level in the following analysis.

282 Figure [23](#) and [Table 3](#) shows the evaluation of model simulation. Driven by
283 observed meteorological and ecological forcings, the CMFD/CSSPv2 simulates
284 monthly streamflow over the Yellow and Yangtze river headwaters quite well.
285 Compared with the observation at Tangnaihai (TNH) and Zhimenda (ZMD) stations,
286 the Kling-Gupta efficiencies of the CMFD/CSSPv2 simulated monthly streamflow are
287 0.94 and 0.91 respectively. The simulated monthly Terrestrial Water Storage Anomaly
288 (TWSA) during 2003-2014 in CMFD/CSSPv2 also agrees with the GRACE satellite
289 observation and captures the increasing trend. For the interannual variations of
290 evapotranspiration, CMFD/CSSPv2 is consistent with the ensemble mean of the
291 GLEAM_ET and MTE_ET products, and the correlation coefficient and root mean
292 squared error (RMSE) during 1982-2011 are 0.87 ($p < 0.01$) and 14 mm/year
293 respectively. This suggests the good performance of the CSSPv2 in simulating the
294 hydrological processes over the Sanjiangyuan region. Although meteorological and
295 ecological outputs from CMIP6 models have coarse resolutions (~100km), the land
296 surface simulation driven by bias corrected CMIP6 results (CMIP6_His/CSSPv2) also
297 captures the terrestrial hydrological variations reasonably well. The Kling-Gupta
298 efficiency of the ensemble mean streamflow simulation reaches up to 0.71~0.81, and
299 the ensemble mean monthly Terrestrial Water Storage Anomaly (TWSA) and annual

300 evapotranspiration generally agree with observations and other reference data
301 (Figures 23c-3d).

302 Figure 34 shows relative changes of terrestrial hydrological variables over the
303 Sanjiangyuan region at different warming levels. The ensemble mean of the increase
304 in annual precipitation is 5% at 1.5°C warming level, and additional 0.5°C and 1.5°C
305 warming will further increase the wetting trends to 7% and 13% respectively. Annual
306 evapotranspiration experiences significant increases at all warming levels, and the
307 ensemble mean increases are 4%, 7% and 13% at 1.5, 2.0 and 3.0°C warming levels
308 respectively. The ratio of transpiration to evapotranspiration also increases
309 significantly, indicating that vegetation transpiration increases much larger than the
310 soil evaporation and canopy evaporation. Although annual total runoff has larger
311 relative changes than evapotranspiration (6%, 9% and 14% at 1.5, 2.0 and 3.0°C
312 warming levels respectively), the uncertainty is large as only 75% of the models show
313 positive signals, which may be caused by large uncertainty in the changes during
314 summer and autumn seasons. The terrestrial water storage (TWS) which includes
315 foliage water, surface water, soil moisture and groundwater, shows slightly decreasing
316 trend at ~~both annual and seasonal scales, however, changes little at the three warming~~
317 ~~levels,~~ suggesting that the increasing precipitation in the future becomes extra
318 evapotranspiration and runoff instead of recharging the local water storage. The
319 accelerated terrestrial hydrological cycle also exists at seasonal scale, as the seasonal
320 changes are consistent with the annual ones.

321 **3.2 Changes in streamflow extremes at different warming levels**

322 Although the intensified terrestrial hydrology induces more streamflow over the
323 headwater region of Yellow river during winter and spring months, streamflow does
324 not increase and even decreases during the flood season (July-September; Figure 45a).
325 Figure 5b shows the changes of streamflow dry extremes over the Yellow river source
326 region at different warming levels, with the error bars showing estimated uncertainties.
327 ~~Moreover,~~ tThe frequency of streamflow dry extremes over the Yellow river is found
328 to increase by 55% at 1.5°C warming level (Figure 45b), but the uncertainty is larger
329 than the ensemble mean. However, suggesting that abnormally low streamflow will
330 occur more frequently during the flood seasons in the future. ~~t~~The dry extreme
331 frequency will further increase to 77% and 125% at the 2.0 and 3.0°C warming levels
332 and the results become are more significant (Figure 45b). No statistically significant
333 changes are found for the wet extremes at all warming levels over the Yellow River
334 headwater region, as the uncertainty ranges are larger than the ensemble means.

335 Over the Yangtze river headwater region, streamflow increases in all months at
336 different warming levels (Figure 45c). The frequency of wet extremes increases
337 significantly by 138%, 202% and 232% at 1.5, 2.0 and 3.0°C warming levels (Figure
338 45d), suggesting a higher risk of flooding. ~~Moreover~~Although, the frequency of dry
339 extremes also tends to decrease significantly by 35%, 44%, 34% at the three warming
340 levels, ~~but~~ the changes are much smaller than those of the wet extremes. Moreover,
341 contributions from climate change and ecological change are both smaller than the
342 uncertainty ranges (not shown), suggesting that their impacts on the changes of dry
343 extremes over the Yangtze river headwater region are not distinguishable. Thus, we

344 mainly focus on the dry extremes over the Yellow river and the wet extremes over the
345 Yangtze river in the following analysis.

346 Different changes of streamflow extremes over the Yellow and Yangtze rivers
347 can be interpreted from different accelerating rates of precipitation and
348 evapotranspiration. Figure 56 shows probability density functions (PDFs) of
349 precipitation, evapotranspiration and their difference (P-ET, i.e. residual water for
350 runoff generation) during the flood season. Over the Yellow river, PDFs of
351 precipitation and evapotranspiration both shift to the right against the reference period,
352 except for the precipitation at 1.5°C warming level. However, the increasing trend of
353 evapotranspiration is stronger than that of precipitation, leading to a left shift of PDF
354 for P-ET. Moreover, increased variations of precipitation and evapotranspiration, as
355 indicated by the increased spread of their PDFs, also lead to a larger spread of PDFs
356 of P-ET. The above two factors together induce a heavier left tail in the PDF of P-ET
357 for the warming future than the reference period (Figure 56e). The probability of
358 P-ET<80mm increases from 0.1 during historical period to 0.11, 0.13 and 0.16 at 1.5,
359 2.0 and 3.0°C warming levels individually. This indicates a higher probability of less
360 water left for runoff generation at different warming levels, given little changes in
361 TWS (section 3.1). Moreover, Figure 36e also shows little change to the right tails in
362 the PDF of P-ET as probability for P-ET>130mm stays around 0.1 (P-ET>130mm) at
363 different warming levels, suggesting little change to the probability of high residual
364 water. This is consistent with the insignificant wet extreme change over the Yellow
365 river. Over the Yangtze river, however, intensified evapotranspirationprecipitation is

366 much ~~larger~~ smaller than the increased ~~evapotranspiration~~ precipitation, leading to a
367 systematic rightward shift of the PDF of P-ET (Figures ~~56b~~, ~~56d~~ and ~~56f~~). Thus both
368 the dry and wet extremes show significant changes over the Yangtze river.

369 **3.3 Influences of land cover change and CO₂ physiological forcing**

370 Figures ~~67a-67b~~ show the changes of streamflow extremes (compared with the
371 reference period) induced by climate and ecological factors. ~~Although the contribution~~
372 ~~from climate change (red bars in Figures 7a-7b) is greater than the ecological factors~~
373 ~~(blue and cyan bars in in Figures 7a-7b), influences of CO₂ physiological forcing and~~
374 ~~land cover change are nontrivial.~~ The CO₂ physiological forcing tends to alleviate dry
375 extremes (or increase wet extremes), while land cover change plays a contrary role.
376 Over the Yellow river, the combined impact of the two ecological factors (sum of blue
377 and cyan bars) reduces the increasing trend of dry extremes caused by climate change
378 (red bars) by 18~22% at 1.5 and 2.0 °C warming levels, while intensifies the dry
379 extremes by 9% at 3.0°C warming level. This can be interpreted from their
380 contributions to the evapotranspiration, as the increased LAI enhancement on ET is
381 weaker than the suppression effect of CO₂ physiological impact at 1.5 and 2.0°C
382 warming levels, while stronger at 3.0°C warming level (not shown). Over the Yangtze
383 river, similarly, combined effect of land cover and CO₂ physiological forcing
384 increases the wet extremes by 9% at 1.5°C warming level while decreases the wet
385 extremes by 12% at 3.0°C warming level. ~~Thus, although contribution from climate~~
386 ~~change is greater than the ecological factors, plays the dominate role in inducing the~~
387 ~~extreme changes at different warming levels, influences of CO₂ physiological forcing~~

388 ~~and land cover change are nontrivial.~~

389 In addition, Figures 67c and 67d show that the combined impact of CO₂
390 physiological forcing and land cover change also influences the differences between
391 different warming levels. Over the Yellow river, climate change increases dry
392 extremes by 26% from 1.5 to 2.0°C warming level, and by 40% from 1.5 and 3.0°C
393 warming level (red bars in Figure 67c). After considering the two ecological factors
394 (pink bars in Figure 67c), above two values change to 22% and 70% respectively, and
395 the difference between 1.5 and 3.0°C warming levels becomes significant. For the wet
396 extreme over the Yangtze river (Figure 67d), the climate change induced difference
397 between 1.5 and 2.0°C warming levels is decreased by 16% after accounting for the
398 two ecological factors. And this decrease reaches up to 49% for the difference
399 between 1.5 and 3.0°C warming levels. We also compared the scenarios when CO₂
400 physiological forcing and land cover change are combined with climate change
401 individually (blue and cyan bars in Figures 67c-d), and the results show the land cover
402 change dominates their combined influences on the difference between different
403 warming levels.

404 **4 Conclusions and Discussion**

405 This study investigates changes of streamflow extremes over the Sanjiangyuan
406 region at different global warming levels through high-resolution land surface
407 modeling driven by CMIP6 climate simulations. The terrestrial hydrological cycle
408 under global warming of 1.5°C is found to accelerate by 4~6% compared with the
409 reference period of 1985-2014, according to the relative changes of precipitation,

410 evapotranspiration and total runoff. The terrestrial water storage, however, shows a
411 slight but significant decreasing trend as increased evapotranspiration and runoff are
412 larger than the increased precipitation. This decreasing trend of terrestrial water
413 storage in the warming future is also found in six major basins in China (Jia et al.,
414 2020). Although streamflow changes during the flood season has a large uncertainty,
415 the frequency of wet extremes over the Yangtze river will increase significantly by
416 138% and that of dry extremes over the Yellow river will increase by 55% compared
417 with that during 1985~2014. With an additional 0.5°C warming, the frequency of dry
418 and wet extremes will increase further by 22~64%. If the global warming is not
419 adequately managed (e.g., to reach 3.0°C), wet extremes over the Yangtze river and
420 dry extremes over the Yellow river will increase by 232% and 125%. ~~These~~
421 nonlineare changes from 1.5 to 2.0 and 3.0°C are nonlinear compared with that from
422 reference period to 1.5°C, which are also found for some fixed-threshold climate
423 indices over the Europe (Dosio and Fischer, 2018). It is necessary to cap the global
424 warming at 2°C or even lower level, to reduce the risk of wet and dry extremes over
425 the Yangtze and Yellow rivers.

426 This study also shows the nontrivial contributions from land cover change and
427 CO₂ physiological forcing to the extreme streamflow changes especially at 2.0 and
428 3.0°C warming levels. The CO₂ physiological forcing is found to increase streamflow
429 and reduce the dry extreme frequency by 14~24%, which is consistent with previous
430 research that CO₂ physiological forcing would increase available water and reduce
431 water stress at the end of this century (Wiltshire et al., 2013). However, our results

432 further show that the drying effect of increasing LAI on streamflow will exceed the
433 wetting effect of CO₂ physiological forcing at 3.0°C warming level (during
434 2048~2075) over the Sanjiangyuan region, making a reversion in the combined
435 impacts of CO₂ physiological forcing and land cover. Thus it is vital to consider the
436 impact of land cover change in the projection of future water stress especially at high
437 warming scenarios.

438 Moreover, about 43~52% of the extreme streamflow changes between 1.5 and
439 3.0°C warming levels are attributed to the increased LAI. Considering the LAI
440 projections from different CMIP6 models are induced by the climate change, it can be
441 inferred that the indirect influence of climate change (e.g., through land cover change)
442 has the same and even larger importance on the changes of streamflow extremes
443 between 1.5 and 3.0°C or even higher warming levels, compared with the direct
444 influence (e.g., through precipitation and evapotranspiration). Thus, it is vital to
445 investigate hydrological and its extremes changes among different warming levels
446 from an eco-hydrological perspective instead of focusing on climate change alone.

447 Although we used 11 CMIP6 models combined with two SSP scenarios to reduce
448 the uncertainty of future projections caused by GCMs, using a single land surface
449 model may result in uncertainties (Marx et al., 2018). However, considering the good
450 performance of the CSSPv2 land surface model over the Sanjiangyuan region and the
451 dominant role of GCMs' uncertainty (Zhao et al., 2019; Samaniego et al., 2017),
452 uncertainty from the CSSPv2 model should have limited influence on the robust of
453 the result.

454

455 **Acknowledgments** We thank the World Climate Research Programme's Working

456 Group on Couple modelling for providing CMIP6 data (<https://esgf-node.llnl.gov>).

457 This work was supported by National Key R&D Program of China

458 (2018YFA0606002) and National Natural Science Foundation of China (41875105,

459 91547103), and the Startup Foundation for Introducing Talent of NUIST.

460

461 **Competing interests**

462 The authors declare that they have no conflict of interest.

463

464 **References**

465 Bibi, S., Wang, L., Li, X., Zhou, J., Chen, D., and Yao, T.: Climatic and associated
466 cryospheric, biospheric, and hydrological changes on the Tibetan Plateau: a
467 review, Int. J. Climatol., 38, e1-e17, <https://doi.org/10.1002/joc.5411>, 2018.

468 Chen, J., Gao, C., Zeng, X., Xiong, M., Wang, Y., Jing, C. Krysanova, V., Huang, J.,
469 Zhao, N., and Su, B.: Assessing changes of river discharge under global warming
470 of 1.5 ° C and 2 ° C in the upper reaches of the Yangtze River Basin: Approach
471 by using multiple-GCMs and hydrological models, Quatern. Int., 453, 1 - 11,
472 <http://dx.doi.org/10.1016/j.quaint.2017.01.017>, 2017.

473 Cuo, L., Zhang, Y., Zhu, F., and Liang, L.: Characteristics and changes of streamflow
474 on the Tibetan Plateau: A review, J. Hydrol.-Reg. Stud., 2, 49 - 68,
475 <https://doi.org/10.1016/j.ejrh.2014.08.004>, 2014.

476 Dai, Y. J., Zeng, X. B., Dickinson, R. E., Baker, I., Bonan, G. B., Bosilovich, M. G.,
477 Denning, A. S., Dirmeyer, P. A., Houser, P. R., Niu, G. Y., Oleson, K. W.,
478 Schlosser, C. A., and Yang, Z. L.: The Common Land Model. B. Am. Meteorol.
479 Soc., 84, 1013 - 1024, <https://doi.org/10.1175/BAMS-84-8-1013>, 2003.

480 Döll, P., Trautmann, T., Gerten, D., Schmied, H. M., Ostberg, S., Saaed, F., and
481 Schleussner, C.: Risks for the global freshwater system at 1.5 ° C and 2 ° C
482 global warming. Environ. Res. Lett., 13, 044038,
483 <https://doi.org/10.1088/1748-9326/aab792>, 2018.

484 Dosio, A., and Fischer, E. M.: Will half a degree make a difference? Robust
485 projections of indices of mean and extreme climate in Europe under 1.5 ° C, 2 °

486 C, and 3 ° C global warming, *Geophys. Res. Lett.*, 45.
487 <https://doi.org/10.1002/2017GL076222>, 2018.

488 Eyring, V., Bony, S., Meehl, G. A., Senior, C. A., Stevens, B., Stouffer, R. J., and
489 Taylor, K. E.: Overview of the Coupled Model Intercomparison Project Phase 6
490 (CMIP6) experimental design and organization, *Geosci. Model Dev.*, 9, 1937 –
491 1958. <https://doi.org/10.5194/gmd-9-1937-2016>, 2016.

492 [Fowler, M. D., Kooperman G. J., Randerson, J. T. and Pritchard M. S.: The effect of](#)
493 [plant physiological responses to rising CO2 on global streamflow, *Nat. Clim.*](#)
494 [*Change*, 9, 873-879, <https://doi.org/10.1038/s41558-019-0602-x>, 2019.](#)

495 He, J., Yang, K., Tang, W., Lu, H., Qin, J., Chen, Y., and Li, X.: The first
496 high-resolution meteorological forcing dataset for land process studies over
497 China, *Sci. Data*, 7, 25. <https://doi.org/10.1038/s41597-020-0369-y>, 2020.

498

499 Hempel, S., Frieler, K., Warszawski, L., and Piontek, F.: A trend-preserving bias
500 correction-the ISI-MIP approach, *Earth Syst. Dyn.*, 4, 219-236.
501 <https://doi.org/10.5194/esd-4-219-2013>, 2013.

502 Ji, P., and Yuan, X.: High-resolution land surface modeling of hydrological changes
503 over the Sanjiangyuan region in the eastern Tibetan Plateau: 2. Impact of climate
504 and land cover change, *J. Adv. Model. Earth. Sy.*, 10, 2829 – 2843.
505 <https://doi.org/10.1029/2018MS001413>, 2018.

506 [Jia, B., Cai, X., Zhao, F., Liu, J., Chen, S., Luo, X., Xie, Z., and Xu, J.: Potential](#)
507 [future changes of terrestrial water storage based on climate projections by](#)

508 [ensemble model simulations, Adv. Water Resour., 142, 103635.](#)
509 <https://doi.org/10.1016/j.advwatres.2020.103635>, 2020.

510 Jung, M., Reichstein, M., and Bondeau, A.: Towards global empirical upscaling of
511 FLUXNET eddy covariance observations: Validation of a model tree ensemble
512 approach using a biosphere model, Biogeosciences, 6, 2001–2013.
513 <https://doi.org/10.5194/bg-6-2001-2009>, 2009.

514 Kuang, X., and Jiao, J.: Review on climate change on the Tibetan Plateau during the
515 last half century, J. Geophys. Res. Atmos., 121, 3979 – 4007.
516 <https://doi.org/10.1002/2015JD024728>, 2016.

517 [Li, J., Liu, D., Li, Y., Wang, S., Yang, Y., Wang, X., Guo, H., Peng, S., Ding, J., Shen,](#)
518 [M., and Wang, L.: Grassland restoration reduces water yield in the headstream](#)
519 [region of Yangtze River, Sci. Rep., 7, 2162,](#)
520 <https://doi.org/10.1038/s41598-017-02413-9>, 2017.

521 Li, W., Jiang, Z., Zhang, X., Li, L. and Sun, Y.: Additional risk in extreme
522 precipitation in China from 1.5 ° C to 2.0 ° C global warming levels, Sci.
523 Bull., 63, 228. <https://doi.org/10.1016/j.scib.2017.12.021>, 2018.

524 Liang, L., Li, L., Liu, C., and Cuo, L.: Climate change in the Tibetan Plateau Three
525 Rivers Source Region: 1960 – 2009, Int. J. Climatol., 33, 2900-2916.
526 <https://doi.org/10.1002/joc.3642>, 2013.

527 [Liang, X., Lettenmaier, D. P., Wood, E. F., and Burges, S. J.: A simple hydrologically](#)
528 [based model of land surface water and energy fluxes for general circulation](#)

529 [models, J. Geophys. Res., 99, 14,415-14,428. https://doi.org/10.1029/94JD00483,](https://doi.org/10.1029/94JD00483)
530 [1994.](https://doi.org/10.1029/94JD00483)

531 Marcott, S. A., Shakun, J. D., Clark, P. U., and Mix, A. C.: A Reconstruction of
532 Regional and Global Temperature for the Past 11,300 Years, *Science*, 339, 1198
533 - 1201. <https://doi.org/10.1126/science.1228026>, 2013.

534 Martens, B., Miralles, D. G., Lievens, H., van der Schalie, R., de Jeu, R. A. M.,
535 Fernández-Prieto, D., Beck, H. E., Dorigo, W. A., and Verhoest, N. E. C.:
536 GLEAM v3: satellite-based land evaporation and root-zone soil moisture, *Geosci.*
537 *Model Dev.*, 10, 1903–1925. <https://doi.org/10.5194/gmd-10-1903-2017>, 2017.

538 Marx, A., Kumar, R., and Thober, S.: Climate change alters low flows in Europe
539 under global warming of 1.5, 2, and 3 ° C, *Hydrol. Earth. Syst. Sc.*, 22, 1017 -
540 1032. <https://doi.org/10.5194/hess-22-1017-2018>, 2018.

541 [Meinshausen, M., Nicholls, Z. R. J., Lewis, J., Gidden, M. J., Vogel, E., Freund, M.,](https://doi.org/10.5194/gmd-13-3571-2020)
542 [Beyerle, U., Gessner, C., Nauels, A., Bauer, N., Canadell, J. G., Daniel, J. S.,](https://doi.org/10.5194/gmd-13-3571-2020)
543 [John, A., Krummel, P. B., Luderer, G., Meinshausen, N., Montzka, S. A., Rayner,](https://doi.org/10.5194/gmd-13-3571-2020)
544 [P. J., Reimann, S., Smith, S. J., van den Berg, M., Velders, G. J. M., Vollmer, M.](https://doi.org/10.5194/gmd-13-3571-2020)
545 [K., and Wang, R. H. J.: The shared socio-economic pathway \(SSP\) greenhouse](https://doi.org/10.5194/gmd-13-3571-2020)
546 [gas concentrations and their extensions to 2500, *Geosci. Model Dev.*, 13, 3571 -](https://doi.org/10.5194/gmd-13-3571-2020)
547 [3605, https://doi.org/10.5194/gmd-13-3571-2020, 2020.](https://doi.org/10.5194/gmd-13-3571-2020)

548 Meinshausen, M., Vogel, E., and Nauels, A., [Lorbacher, K., Meinshausen, N.,](https://doi.org/10.5194/gmd-13-3571-2020)
549 [Etheridge, D. M., Fraser, P. J., Montzka, S. A., Rayner, P. J., Trudinger, C. M.,](https://doi.org/10.5194/gmd-13-3571-2020)
550 [Krummel, P. B., Beyerle, U., Canadell, J. G., Daniel, J. S., Enting, I. G., Law, R.](https://doi.org/10.5194/gmd-13-3571-2020)

551 [M., Lunder, C. R., O'Doherty, S., Prinn, R. G., Reimann, S., Rubino, M., Velders,](#)
552 [G. J. M., Vollmer, M. K., Wang, R. H. J., and Weiss, R.:](#) Historical greenhouse
553 gas concentrations for climate modelling (CMIP6), *Geosci. Model Dev.*, 10,
554 2057-2116. <https://doi.org/10.5194/gmd-10-2057-2017>, 2017.

555 Mohammed, K., Islam, A. S., Islam, G. M. T., Alfieri, L., Bala, S. K., and Khan, M. J.
556 U.: Extreme flows and water availability of the Brahmaputra River under 1.5 and
557 2 ° C global warming scenarios, *Climatic Change*, 145, 159-175.
558 <https://doi.org/10.1007/s10584-017-2073-2>, 2017.

559 Morice, C. P., Kennedy J. J., Rayner N. A., and Jones P. D.: Quantifying uncertainties
560 in global and regional temperature change using an ensemble of observational
561 estimates: The HadCRUT4 dataset, *J. Geophys. Res.*, 117, D08101.
562 <https://doi.org/10.1029/2011JD017187>, 2012.

563 [Oleson, K. W., Lawrence, D. M., Bonan, G. B., Drewniak, B., Huang, M., Koven, C.](#)
564 [D., Levis, S., Li, F., Riley, W. J., Subin, Z. M., Swenson, S. C., Thornton, P. E.,](#)
565 [Bozbiyik, A., Fisher, R., Heald, C. L., Kluzek, E., Lamarque, J. F., Lawrence, P.](#)
566 [J., Leung, L. R., Lipscomb, W., Muszala, S., Ricciuto, D. M., Sacks, W., Sun, Y.,](#)
567 [Tang, J., Yang, Z. L.: Technical description of version 4.5 of the Community](#)
568 [Land Model \(CLM\) \(Rep. NCAR/TN-503 + STR, 420\), 2013.](#)

569 O'Neill, B. C., Tebaldi, C., Vuuren, D. P. V., Eyring, V., Friedlingstein, P., Hurtt, G.,
570 Knutti, R., Kriegler, E., Lamarque, J. F., Lowe, J., Meehl, G. A., Moss, R., Riahi,
571 K., and Sanderson, B. M.: The scenario model intercomparison project

572 (ScenarioMIP) for CMIP6, Geosci. Model Dev., 9, 3461-3482.
573 <https://doi.org/10.5194/gmd-9-3461-2016>, 2016.

574 [Samaniego, L., Kumar, R., Breuer, L., Chamorro, A., Flörke, M., Pechlivanidis, I. G.,
575 Schäfer, D., Shah, H., Vetter, T., Wortmann, M., and Zeng, X.: Propagation of
576 forcing and model uncertainties on to hydrological drought characteristics in a
577 multi-model century-long experiment in large river basins, Climatic Change, 141,
578 435-449. <https://doi.org/10.1007/s10584-016-1778-y>, 2017.](#)

579 Thober, T., Kumar, R., and Waders, N.: Multi-model ensemble projections of
580 European river floods and high flows at 1.5, 2, and 3 degrees global warming,
581 Environ. Res. Lett., 13, 014003. <https://doi.org/10.1088/1748-9326/aa9e35>,
582 2018.

583 Vicente-Serrano, S. M., Lopez-Moreno, J. I., Begueria, S., Lorenzo-Lacruz, J.,
584 Azorin-Molina, C., and Moran-Tejeda, E.: Accurate computation of a streamflow
585 drought index, J. Hydrol. Eng., 17, 318 - 332.
586 [https://doi.org/10.1061/\(Asce\)He.1943-5584.0000433](https://doi.org/10.1061/(Asce)He.1943-5584.0000433), 2012.

587 Watkins, M. M., Wiese, D. N., Yuan, D. N., Boening, C., and Landerer, F. W.:
588 Improved methods for observing Earth's time variable mass distribution with
589 GRACE using spherical cap mascons, J. Geophys. Res. Solid Earth, 120,
590 2648-2671. <https://doi.org/10.1002/2014JB011547>, 2015.

591 Wiltshire, A., Gornall, J., Booth, B., Dennis, E., Falloon, P., Kay, G., McNeall, D.,
592 McSweeney, C. and Betts, R.: The importance of population, climate change and
593 CO2 plant physiological forcing in determining future global water stress, Global

594 Environ. Change, 23(5), 1083-1097.
595 <http://dx.doi.org/10.1016/j.gloenvcha.2013.06.005>, 2013.

596 WMO.: WMO Statement on the State of the Global Climate in 2019,
597 https://library.wmo.int/doc_num.php?explnum_id=10211, 2020.

598 Yang, K., Wu, H., Qin, J., Lin, C., Tang, W., and Chen, Y.: Recent climate changes
599 over the Tibetan plateau and their impacts on energy and water cycle: A review,
600 Global Planet. Change, 112, 79 – 91.
601 <https://doi.org/10.1016/j.gloplacha.2013.12.001>, 2013.

602 Yang, Y., Rodericj, M. L., Zhang, S., McVicar, T. R., and Donohue, R. J.: Hydrologic
603 implications of vegetation response to elevated CO2 in climate projections, Nat.
604 Clim. Change, 9, 44-48. <https://doi.org/10.1038/s41558-018-0361-0>, 2019.

605 Yuan, X., Ji, P., Wang, L., Liang, X., Yang, K., Ye, A., Su, Z., and Wen, J.: High
606 resolution land surface modeling of hydrological changes over the Sanjiangyuan
607 region in the eastern Tibetan Plateau: 1. Model development and evaluation, J.
608 Adv. Model. Earth. Sy., 10, 2806 – 2828. <https://doi.org/10.1029/2018MS001413>,
609 2018a.

610 Yuan, X., Jiao, Y., Yang, D., and Lei, H.: Reconciling the attribution of changes in
611 streamflow extremes from a hydroclimate perspective, Water Resour. Res., 54,
612 3886 – 3895. <https://doi.org/10.1029/2018WR022714>, 2018b.

613 Yuan, X., Zhang, M., Wang, L., and Zhou, T.: Understanding and seasonal forecasting
614 of hydrological drought in the Anthropocene, Hydrol. Earth. Syst. Sc., 21, 5477
615 – 5492. <https://doi.org/10.5194/hess-21-5477-2017>, 2017.

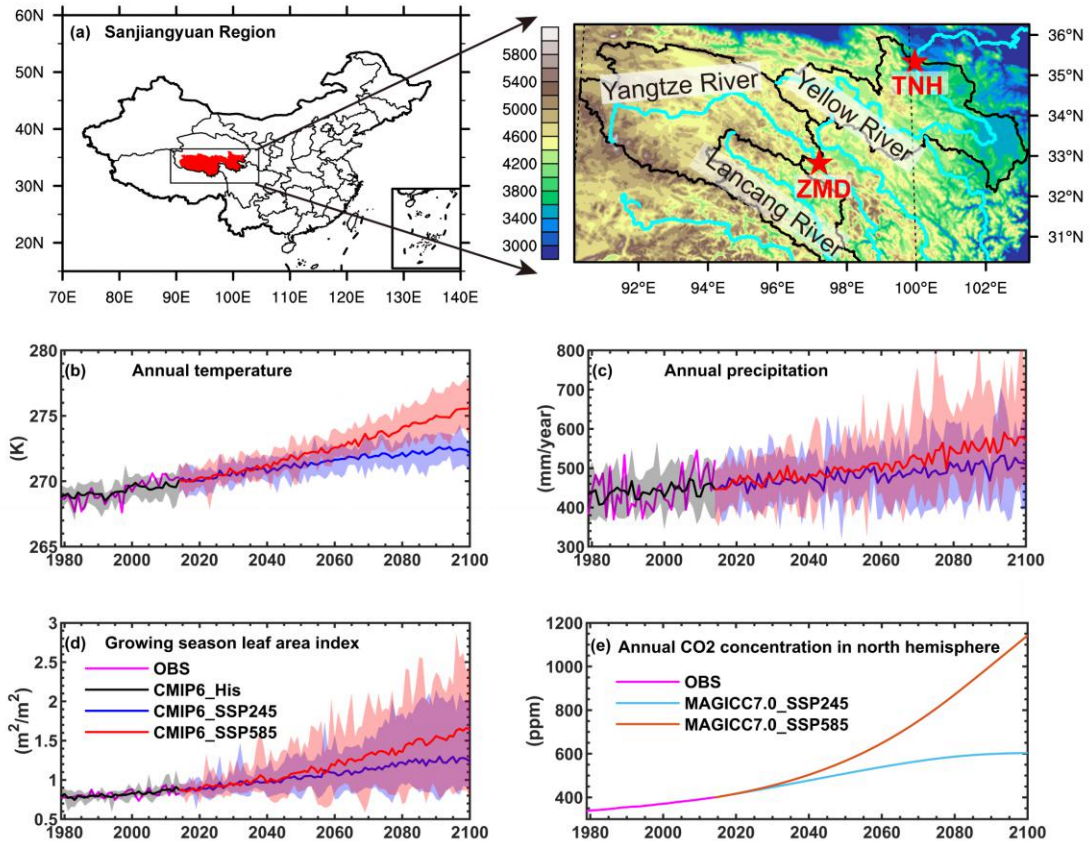
616 Zhang Y., You Q., Chen C., and Ge J.: Impacts of climate change on streamflows
617 under RCP scenarios: A case study in Xin River Basin, China, Atmos. Res.,
618 178-179, 521-534. <http://dx.doi.org/10.1016/j.atmosres.2016.04.018>, 2016.

619 Zhao Q., Ding Y., Wang J., Gao H., Zhang S., Zhao C. Xu J. Han H., and Shangguan
620 D.: Projecting climate change impacts on hydrological processes on the Tibetan
621 Plateau with model calibration against the glacier inventory data and observed
622 streamflow, J. Hydrol., 573, 60-81. <https://doi.org/10.1016/j.jhydrol.2019.03.043>,
623 2019.

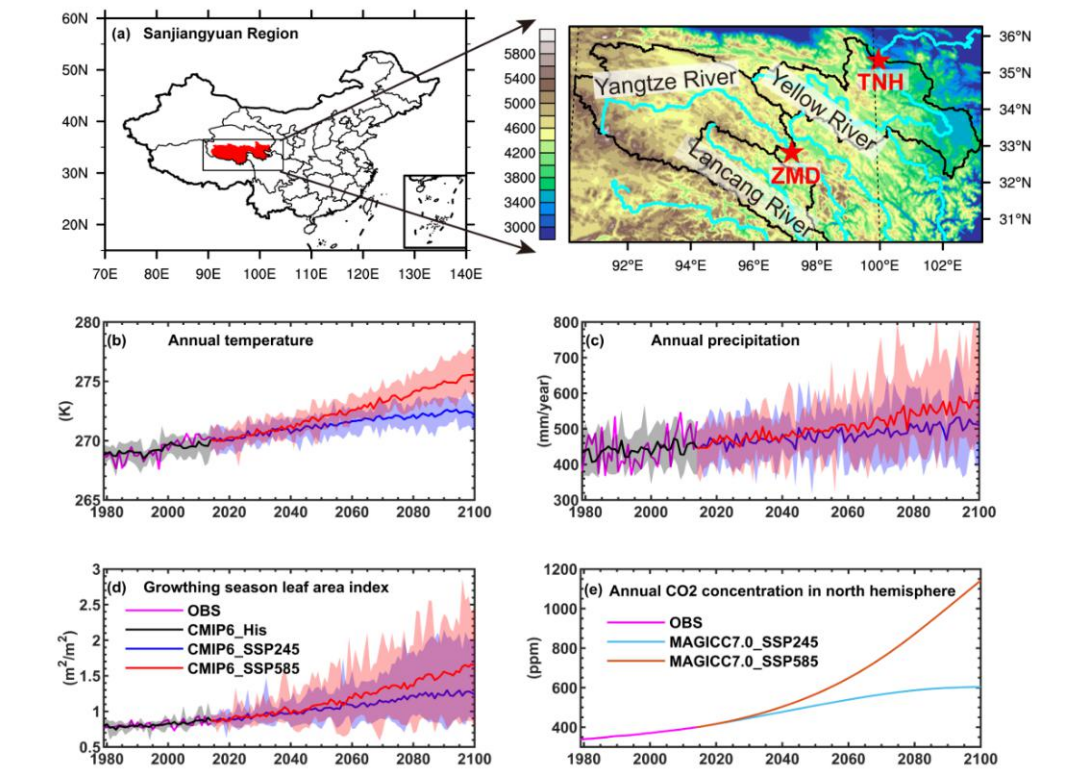
624 Zhu Q., Jiang H., Peng C., Liu J., Fang X., Wei X., Liu S., and Zhou G.: Effects of
625 future climate change, CO2 enrichment, and vegetation structure variation on
626 hydrological processes in China, Global Planet. Change, 80-81, 123-135.
627 <https://doi.org/10.1016/j.gloplacha.2011.10.010>, 2012.

628 [Zhu, Z. C., Piao, S. L., Myneni, R. B., Huang, M. T., Zeng, Z. Z., Canadell, J. G.,](#)
629 [Ciais, P., Sitch, S., Friedlingstein, P., Arneeth, A., Cao, C. X., Cheng, L., Kato, E.,](#)
630 [Koven, C., Li, Y., Lian, X., Liu, Y. W., Liu, R. G., Mao, J. F., Pan, Y. Z., Peng, S.](#)
631 [S., Penuelas, J., Poulter, B., Pugh, T. A. M., Stocker, B. D., Viovy, N., Wang, X.](#)
632 [H., Wang, Y. P., Xiao, Z. Q., Yang, H., Zaehle, S., and Zeng, N.: Greening of the](#)
633 [Earth and its drivers, Nature Climate Change, 6\(8\), 791-+,](#)
634 <https://doi.org/10.1038/Nclimate3004>, 2016.

635



636



637

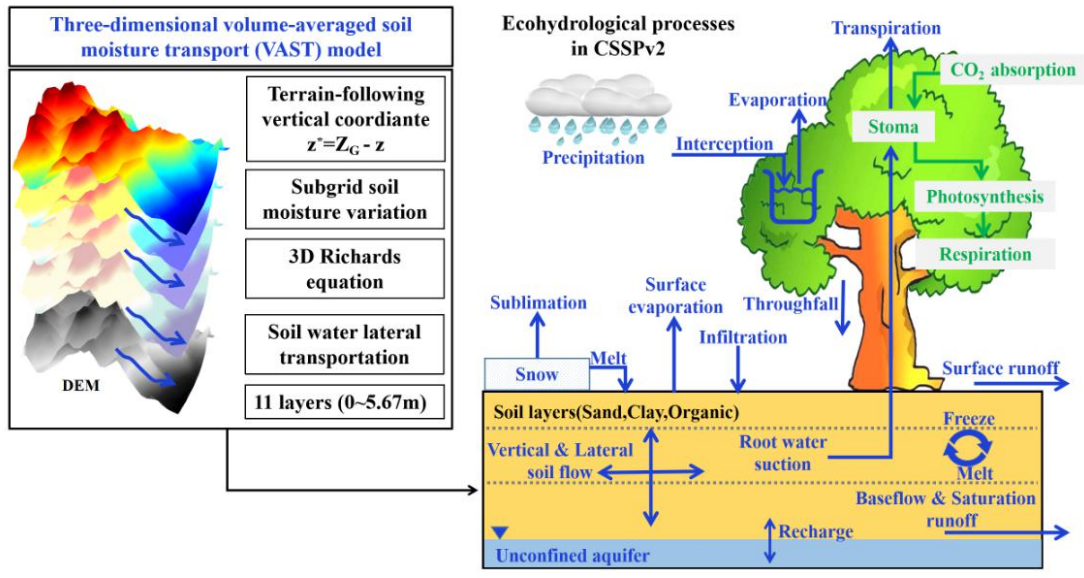
638 **Figure 1.** (a) The locations of the Sanjiangyuan region and streamflow gauges. (b)-(e)

639 are the time series of annual temperature, precipitation, growing season leaf area

640 index and CO₂ concentration averaged over the Sanjiangyuan region during
641 1979-2100. Red pentagrams in (a) are two streamflow stations named Tangnaihai
642 (TNH) and Zhimenda (ZMD). Black, blue and red lines in (b-d) are ensemble means
643 of CMIP6 model simulations from the historical, SSP245 and SSP585 experiments.
644 Shadings are ranges of individual ensemble members. Cyan and brown lines in (e) are
645 future CO₂ concentration under SSP245 and SSP585 scenarios simulated by
646 MAGICC7.0 model.

647

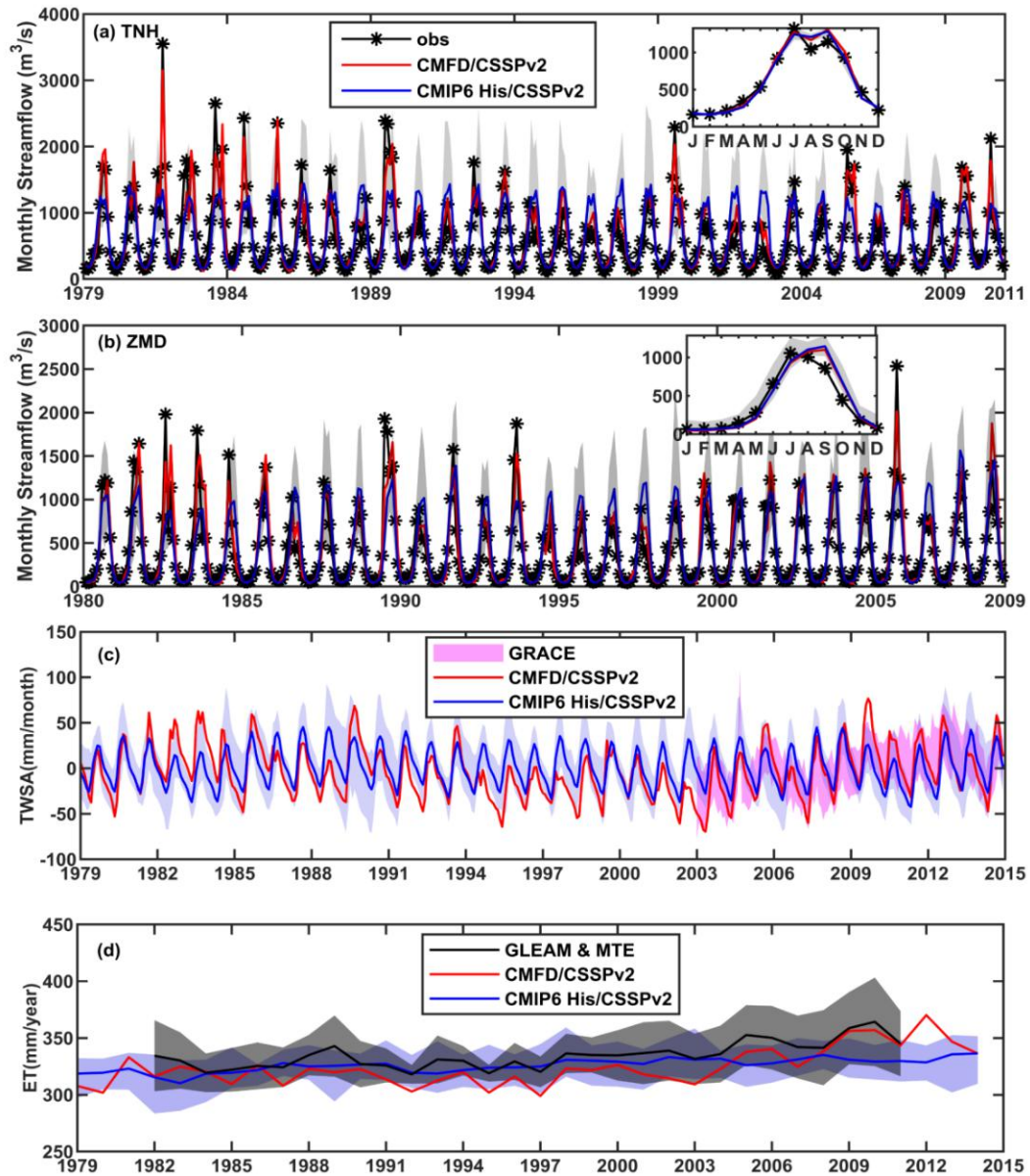
648



649

650 **Figure 2. Main ecohydrological processes in the Conjunctive Surface-Subsurface**

651 **Process version 2 (CSSPv2) land surface model.**



652

653 **Figure 23.** Evaluation of model simulations. (a-b) Observed and simulated monthly

654 streamflow at the Tangnaihai (TNH) and Zhimenda (ZMD) hydrological stations, with

655 the climatology shown in the upper-right corner. (c-d) Evaluation of the simulated

656 monthly terrestrial water storage anomaly (TWSA) and annual evapotranspiration (ET)

657 averaged over the Sanjiangyuan region. Red lines are CSSPv2 simulation forced by
 658 observed meteorological forcing. Blue lines represent ensemble means of 11

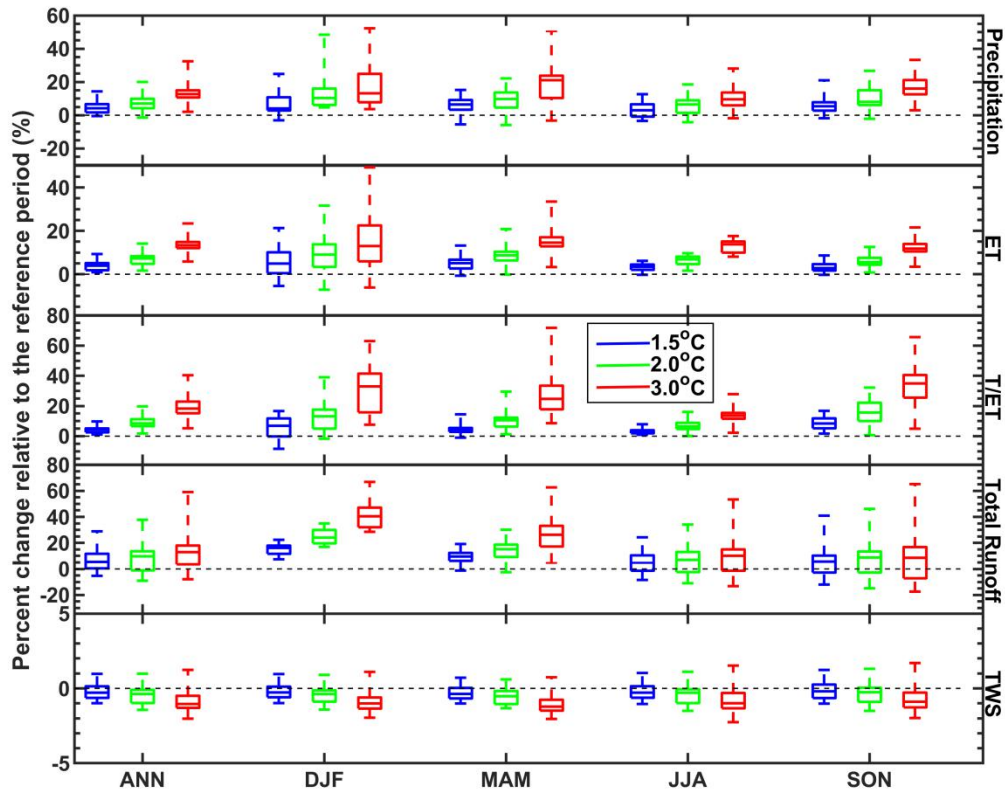
659 CMIP6_His/CSSPv2 simulations, while gray shadings in (a-b) and blue shadings in

660 (c-d) are ranges of individual ensemble members. Pink shading in (c) is GRACE

661 satellite observations. Black line and black shading in (d) are ensemble mean and
662 ranges of GLEAM_ET and MTE_ET datasets.

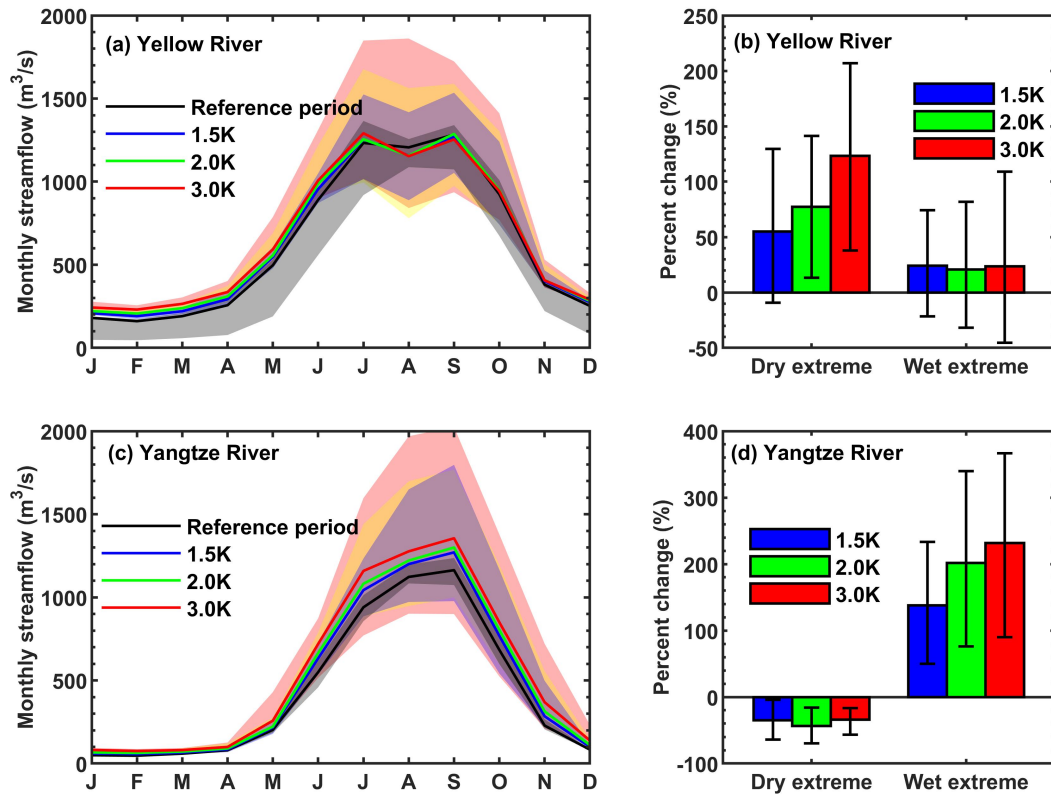
663

664



665

666 **Figure 34.** Box plots of relative changes of regional mean precipitation,
 667 evapotranspiration (ET), ratio of transpiration to evapotranspiration (T/ET), total
 668 runoff and terrestrial water storage (TWS) at different global warming levels.
 669 Reference period is 1985-2014, and annual (ANN) and seasonal (winter: DF, spring:
 670 MAM, summer: JJA and autumn: SON) results are all shown. Boxes show 25th to
 671 75th ranges among 22 CMIP6_SSP/CSSPv2 simulations, while lines in the boxes are
 672 median values.



674

675 **Figure 45.** Changes of streamflow and its extremes at the outlets of the headwater

676 regions of the Yellow river and the Yangtze river, i.e., Tangnaihai gauge and

677 Zhimenda gauge. (a) Simulated monthly streamflow ~~climatology~~ over the Yellow

678 river during the reference period (1985-2014) and the periods with different global

679 warming levels. Solid lines represent ensemble means, while shadings are ranges of

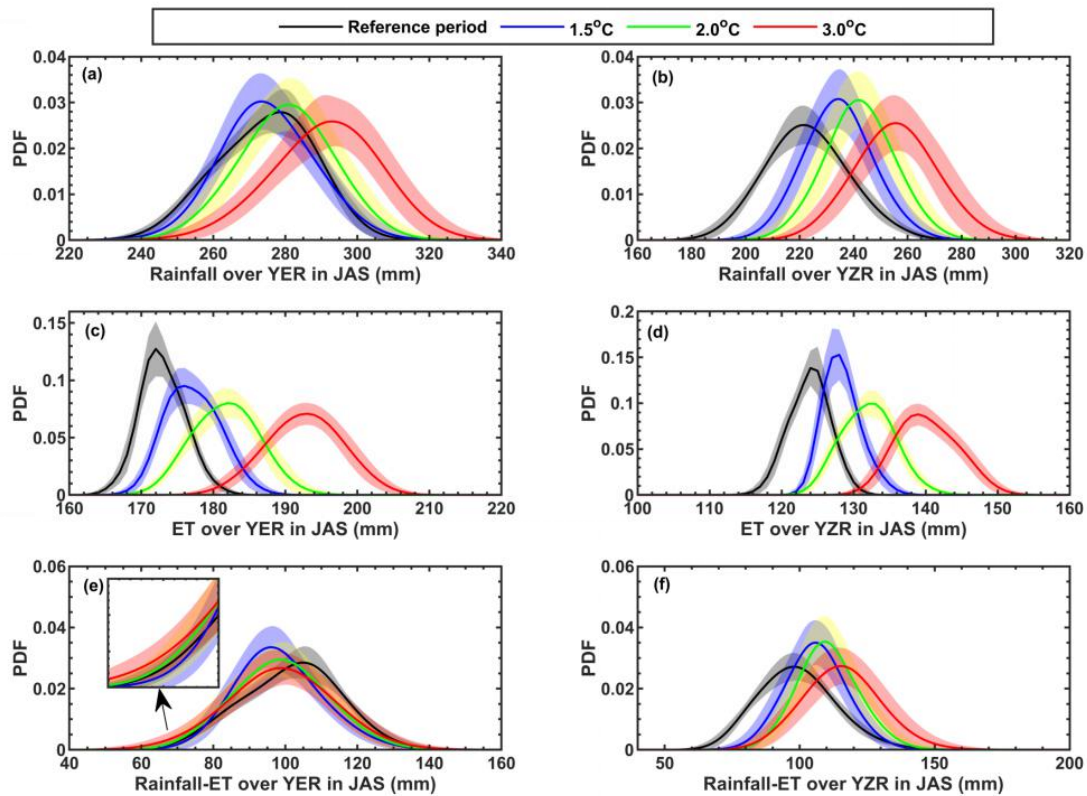
680 individual ensemble members. (b) Percent changes in frequency of dry and wet

681 extremes in July-September at different warming levels. Colored bars are ensemble

682 means, while error bars are 5~95% uncertainty ranges estimated by using

683 bootstrapping for 10,000 times. (c) and (d) are the same as (a) and (b), but for the

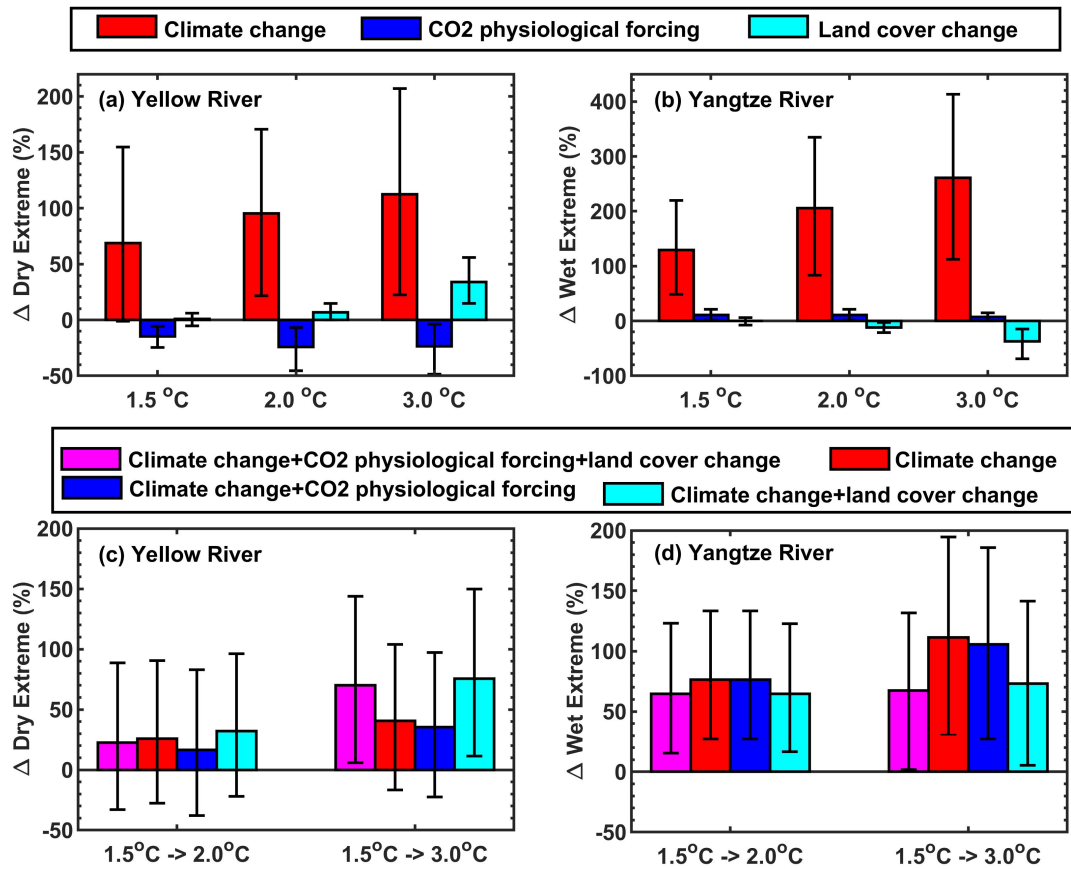
684 Yangtze river.



686

687 **Figure 56.** Probability density functions (PDFs) of regional mean rainfall,
 688 evapotranspiration (ET) and their difference over the headwater regions of Yellow
 689 river (YER) and Yangtze river (YZR) during flooding seasons (July-September) for
 690 the reference period (1985-2014) and the periods with 1.5, 2.0 and 3.0°C global
 691 warming levels. Shadings are 5~95% uncertainty ranges.

692



693

694 **Figure 67.** (a-b) Influences of climate change, CO₂ physiological forcing and land
 695 cover change on relative changes in frequency of the dry and wet extremes in
 696 July-September at different global warming levels for the headwater regions of
 697 Yellow river and Yangtze river. (c-d) Changes of dry and wet extremes under
 698 additional warming of 0.5°C and 1.5°C with the consideration of different factors. All
 699 the changes are relative to the reference period (1985-2014). Ensemble means are
 700 shown by colored bars while the 5~95% uncertainty ranges estimated by using
 701 bootstrapping for 10,000 times are represented by error bars.

702

703 **Table 1.** CMIP6 simulations used in this study. His means historical simulations
704 during 1979-2014 with both anthropogenic and natural forcings, SSP245 and SSP585
705 represent two Shared Socioeconomic Pathways during 2015-2100. Note the
706 CNRM-CM6-1 and CNRM-ESM2-1 do not provide r1ilp1f1 realization, so r1ilp1f2
707 was used instead.

No.	Models	Experiments	Realization	Horizontal Resolution (Longitude × Latitude Grid Points)
1	ACCESS-ESM1-5	His/SSP245/SSP585	r1ilp1f1	192×145
2	BCC-CSM2-MR	His/SSP245/SSP585	r1ilp1f1	320×160
3	CESM2	His/SSP245/SSP585	r1ilp1f1	288×192
4	CNRM-CM6-1	His/SSP245/SSP585	r1ilp1f2	256×128
5	CNRM-ESM2-1	His/SSP245/SSP585	r1ilp1f2	256×128
6	EC-Earth3-Veg	His/SSP245/SSP585	r1ilp1f1	512×256
7	FGOALS-g3	His/SSP245/SSP585	r1ilp1f1	180×80
8	GFDL-CM4	His/SSP245/SSP585	r1ilp1f1	288×180
9	INM-CM5-0	His/SSP245/SSP585	r1ilp1f1	180×120
10	MPI-ESM1-2-HR	His/SSP245/SSP585	r1ilp1f1	384×192
11	MRI-ESM2-0	His/SSP245/SSP585	r1ilp1f1	320×160

708

709 **Table 2.** Determination of “crossing years” for the periods reaching 1.5, 2 and 3°C
 710 warming levels for different GCM and SSP combinations.

Models	1.5°C warming level		2.0°C warming level		3.0°C warming level	
	SSP245	SSP585	SSP245	SSP585	SSP245	SSP585
ACCESS-ESM1-5	2024	2023	2037	2034	2070	2052
BCC-CSM2-MR	2026	2023	2043	2034	Not found	2054
CESM2	2024	2022	2037	2032	2069	2048
CNRM-CM6-1	2032	2028	2047	2039	2075	2055
CNRM-ESM2-1	2030	2026	2049	2039	2075	2058
EC-Earth3-Veg	2028	2023	2044	2035	2072	2053
FGOALS-g3	2033	2032	2063	2046	Not found	2069
GFDL-CM4	2025	2024	2038	2036	2073	2053
INM-CM5-0	2031	2027	2059	2038	Not found	2063
MPI-ESM1-2-HR	2032	2030	2055	2044	Not found	2066
MRI-ESM2-0	2024	2021	2038	2030	2074	2051

711

712 Table 3. Performance for CSSPv2 model simulations driven by the observed
 713 meteorological forcing (CMFD/CSSPv2) and the bias-corrected CMIP6 historical
 714 simulations (CMIP6_His/CSSPv2). The metrics include correlation coefficient (CC),
 715 root mean squared error (RMSE), and Kling-Gupta efficiency (KGE). The KGE is
 716 only used to evaluate streamflow.

<u>Variables</u>	<u>Experiments</u>	<u>CC</u>	<u>RMSE</u>	<u>KGE</u>
<u>Monthly streamflow at TNH</u>	<u>CMFD/CSSPv2</u>	<u>0.95</u>	<u>165 m³/s</u>	<u>0.94</u>
<u>station</u>	<u>CMIP6_His/CSSPv2</u>	<u>0.76</u>	<u>342 m³/s</u>	<u>0.71</u>
<u>Monthly streamflow at ZMD</u>	<u>CMFD/CSSPv2</u>	<u>0.93</u>	<u>169 m³/s</u>	<u>0.91</u>
<u>station</u>	<u>CMIP6_His/CSSPv2</u>	<u>0.82</u>	<u>257 m³/s</u>	<u>0.81</u>
<u>Monthly terrestrial water</u>	<u>CMFD/CSSPv2</u>	<u>0.7</u>	<u>22 mm/month</u>	<u>-</u>
<u>storage anomaly over the</u>	<u>CMIP6_His/CSSPv2</u>	<u>0.4</u>	<u>24 mm/month</u>	<u>-</u>
<u>Sanjiangyuan region</u>				
<u>Annual evapotranspiration</u>	<u>CMFD/CSSPv2</u>	<u>0.87</u>	<u>14 mm/year</u>	<u>-</u>
<u>over the Sanjiangyuan region</u>	<u>CMIP6_His/CSSPv2</u>	<u>0.47</u>	<u>13 mm/year</u>	<u>-</u>

717

718